pp 1425–1441. © Royal Aeronautical Society 2018
doi: 10.1017/aer.2018.79

A 3D particle model for the plume CEX simulation

C. Lu*, P. Qiu and Y. Cao
yongc@hit.edu.cn
Harbin Institute of Technology
Shenzhen Graduate School
Shenzhen
P.R. China

T.P. Zhang* and J.J. Chen
Lanzhou Institute of Physics
Lanzhou
P.R. China

ABSTRACT

Charge Exchange (CEX) ion is the main factor causing the plume pollution. The distribution of CEX ions is determined by the distribution of beam ions and neutral atoms. Hence, the primary problem in the study of the plume is how to accurately simulate the distribution of beam ions and neutral atoms. At present, the most commonly used model utilised for the plume simulation is the analytical model proposed by Roy for the plume simulation of the NASA Solar Technology Application Readiness (NSTAR) ion thruster. However, this analytical model can only be applied to the ion beam with small divergence angles. In addition, the analytical model is no longer applicable to the simulation for the plume of a new type of ion thruster that appeared recently, which is called the annular ion thruster. In this paper, a 3D particle model is proposed for the plume simulation of ion thrusters consisting of the particle model for beam ions, the Direct Simulation Monte Carlo (DSMC) model for neutral atoms and the Immersed Finite Element-Particle In Cell-Monte Carlo Collision (IFE-PIC-MCC) model for CEX ions. Then, the plume of the NSTAR ion thruster is simulated by both Roy's model and the 3D particle model. The simulation results of both models are then compared with the experimental results. It is shown that the numerical results of the 3D particle model agree well with those of the analytical model and the experimental data. And this 3D particle model can also be used for other electric thrusters.

Keywords: Ion thruster; plume; 3D particle model; IFE-PIC-MCC

* These authors equally contributed to the work

Received 26 January 2018; revised 2 June 2018; accepted 4 June 2018; first published online 17 July 2018.

https://doi.org/10.1017/aer.2018.79 Published online by Cambridge University Press

1.0 INTRODUCTION

Because of the advantages of electric thrusters, such as small size and large specific impulse, the electric thruster is being widely used in the field of satellite communications and deep space explorations. However, in practical applications, it is found that the electric thruster plume will bring great harm to the spacecraft, and even lead to spacecraft failure. For example, Charge Exchange (CEX) ions of the plume can bring thermal loads and pollute electronic components of the spacecraft[1-3]. Therefore, how to reduce the impact of the plume on the spacecraft is critical to the future application of electric thrusters. The research method of the electric thruster plume mainly includes experimental research and numerical simulation. Experiments are time consuming and expensive. Conversely, numerical simulation, which has been widely used, is costly efficient and well adapted. In addition, a further comprehensive understanding of the characteristics of the plume can be obtained.

The composition of the electric thruster plume consists mainly of beam ions, neutral atoms, and CEX ions[4]. The distribution of CEX ions is determined by the distributions of beam ions and neutral atoms. Therefore, how to accurately simulate the distributions of beam ions and neutral atoms is the primary problem of the numerical simulation. The numerical models simulating the distribution of beam ions and neutral atoms include the analytical model and the particle model. The analytical model proposed by Roy[5] is one of the current simulation models of the ion thruster plume. In this model, the beam distribution formula is based on the experimental data. The distribution of neutral atoms is based on the point source model proposed by Bird[6]. And the CEX collision is simulated by Stand Monte Carlo Collision (MCC). Based on the analytical model and the Immersed Finite Element (IEF) methods, Wang[7] simulated the plume of the NASA Solar Technology Application Readiness (NSTAR) ion thruster and then compared the simulation results with the experimental data. It was shown that the simulation results of the analytical model are in good agreement with the experimental data. The analytic model has the advantages like fast calculation and good agreement with the experimental data; but for the case where the divergence angle is too large, or for the plume of other electric thrusters, such as the annular ion thruster[8], the analytic model is no longer applicable. In contrast with the analytical model, the distribution of beam ions and neutral atoms in the particle model are obtained by tracking microscopic particles directly, so its universality is better. For example, Han[9] improved the Mo source model for the ion thruster plume contamination by using the particle model. Wang[10] applied Direct Simulation Monte Carlo (DSMC) and Particle-In-Cell (PIC) simulations to study the effect of the ambient in a vacuum chamber on the potential of the plume. However, the particle model is mainly proposed for Hall thrusters[11-13], so there is no systematic comparison between the analytical model and the particle model for the correctness, accuracy and applicability of the particle model.

Therefore, this paper presents a 3D particle model for the plume of ion thrusters, including the particle model for beam ions, the DSMC model for neutral atoms and the Immersed Finite Element-Particle In Cell-Monte Carlo Collision (IFE-PIC-MCC)[14-17] model for CEX ions. The comparison between the 3D particle model, the analytical model, and the experiment is also done to verify the correctness and accuracy of the 3D particle model. On this basis, the plume of the annular ion thruster is simulated. In the second section, the beam ion sub-models of the analytical model and the 3D particle model are introduced, respectively. Then, the beam ion simulation results of these two models are compared. In the third section, the CEX ion simulation processes of the analytical model and the 3D particle model are illustrated. Then, the simulation results of these two models and the experimental data of the NSTAR ion thruster plume are compared. In the fourth section, the plume of the annular ion thruster

https://doi.org/10.1017/aer.2018.79 Published online by Cambridge University Press

is simulated. It is shown that the simulation results of the 3D particle model are in good agreement with those of the analytical model and the experimental data. Furthermore, the 3D particle model is also applicable for the simulation of the plume of the annular ion thruster and the Hall thruster. In addition, due to the advantage that the IFE methods can quickly deal with complex boundaries in the structured mesh, the 3D particle model also has the potential to calculate the non-axisymmetric plume and to directly calculate the interaction between the plume CEX ion and the complex surface of the spacecraft.

2.0 BEAM ION SIMULATION MODEL

Because of the limitation of the analytical model, we proposed the 3D particle model to cope with the simulation of the plume of new type ion thrusters. In the 3D particle model, the initial problem is how to define the beam ion density distribution, as well as their velocity direction in the outlet plane. Therefore, we discussed these problems in detail. Since the beam ion density distribution of the 3D particle model referred to the analytical model, we first briefly recall the analytical model below.

2.1 Analytical model

As shown in Fig. 1, the beam ion distribution conforms to the point source model. Beam ions are assumed to be emitted from the center of the optics sphere, and the beam current density j_{bi} is the parabolic distribution near the axis and is the exponential distribution in the wing area. And the distribution equation of beam ions in the polar coordinate system is shown in Equation (1)[5].

$$j_{bi}(R,\theta)=\begin{cases} ev_{bi}n_{bi0}\left(\frac{R_c}{R}\right)^2\left(1-\frac{\theta^2}{\alpha^2}\right), & \theta<\gamma\alpha \\ ev_{bi}n_{bi0}\exp\left(-\frac{R\cdot\sin\theta}{\lambda}\right)\left(\frac{R_c}{R}\right)^2\left(1-\frac{\theta^2}{\alpha^2}\right), & \theta\geq\gamma\alpha, \end{cases} \quad \ldots(1)$$

where θ is the angle between the outlet axis of the thruster and the straight line which connects an arbitrary point in the plume region and the center of the optics sphere. When $\theta<\gamma\alpha$, the beam current density distribution is approximately parabolic along the radial direction. When $\theta\geqslant\gamma\alpha$, the beam current density distribution is attenuated by a factor $\exp(-\frac{R\cdot\sin\theta}{\lambda})$, where λ is a decay length scale so that it becomes exponential along the radial direction. Typically, γ

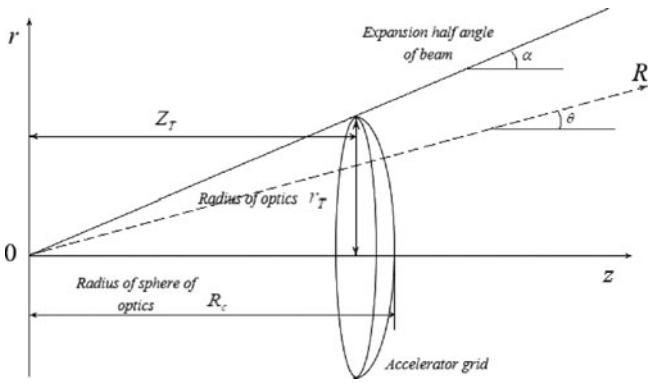
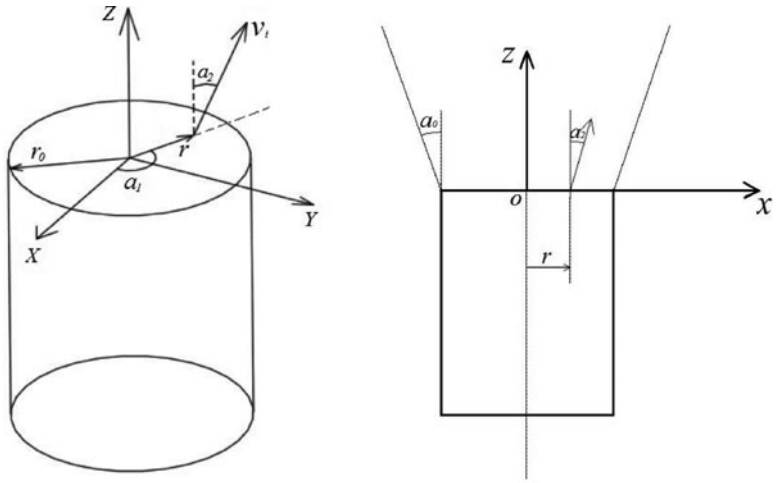


Figure 1. Schematic diagram of beam point source model.

https://doi.org/10.1017/aer.2018.79 Published online by Cambridge University Press



(a) XYZ 3D image (b) XZ 2D section image

Figure 2. The spherical coordinates describing the velocity direction distribution of beam ions.

is valued as 0.95. e is the quantity of electron charge. α is the divergence angle of the beam. R is the distance between the arbitrary point in the plume region and the center of the optics sphere. R_c is the radius of the optics sphere and $R_c \approx r_T/\alpha \cos(\alpha/2)$, where r_T is the radius of optics. n_{bi0} is the density at the center of the thruster outlet. v_{bi}, which is assumed as a constant, is the beam ion velocity:

$$v_{bi} = \sqrt{\frac{2eU_{acc}}{m_i}}, \qquad \ldots (2)$$

where U_{acc} is the accelerating voltage of optics and m_i is the beam ion mass.

2.2 Particle model

As had been mentioned before, in the particle model, the two main things to be determined are the velocity direction and the distribution of the beam ions in the outlet plane.

2.2.1 Velocity direction

The beam ion velocity v_{bi} in the particle model is also calculated by Equation (2) and its direction varies along the radius. As shown in Fig. 2, the initial velocity direction of beam ions can be expressed as (v_i; α_1; α_2) in spherical coordinates, where α_1 is a random number between $0 \sim 2\pi$ and α_2 is varied in accordance to the radial position between $0 \sim \alpha_o$:

$$\alpha_2(r) = \arctan\left(\frac{\tan\alpha_o}{r_o} r\right), \qquad \ldots (3)$$

where α_o is the divergence angle, r_o is the outlet radius of the thruster and r is the distance between the position of a beam ion in the outlet plane and the outlet center.

https://doi.org/10.1017/aer.2018.79 Published online by Cambridge University Press

2.2.2 Density distribution

(1) Parabola distribution

The beam ion density of traditional ion thrusters is high at the outlet center and low at the outlet edge[18], so the density of beam ions n_i shall be determined by Equation (1). Since the wing area is narrow and the beam ion density is also small in the wing area[19], the wing area is neglected in the particle model. In addition, because the average beam ion density is easy to standardise, the n_i can be expressed as the following equation:

$$n_i(r) = A\bar{n}_{bi}\cos^2(\alpha_2(r))\left(1 - \frac{{\alpha_2}^2(r)}{{\alpha_o}^2}\right), \quad \ldots(4)$$

where $\bar{n}_{bi}$ is the average beam ion density, $\bar{n}_{bi} = \frac{I_b}{ev_{bi}\pi r_0^2}$ and I_b is the beam current. A is a correction factor to allow for the continuity.

The beam current I_b in the exit plane of ion thrusters shall meet:

$$I_b = \int_0^{r_0} n_i(r) e v_{bi} 2\pi r \cos(\alpha_2(r)) dr \quad \ldots(5)$$

Substitute Equation (4) into Equation (5) and obtain:

$$I_b = 2Aev_{bi}\bar{n}_{bi}\pi r_0^2 \cdot \frac{1}{\tan^2\alpha_0}\left(1 - \frac{2\cos\alpha_0}{{\alpha_0}^2} - \frac{2\sin\alpha_0}{\alpha_0} + \frac{2}{{\alpha_0}^2}\right) \quad \ldots(6)$$

Let $\delta = (1 - \frac{2\cos\alpha_0}{{\alpha_0}^2} - \frac{2\sin\alpha_0}{\alpha_0} + \frac{2}{{\alpha_0}^2})/(\tan^2\alpha_0)$. When $\alpha_o \ll 1$, $\delta \approx 0.25$ and $A \approx 2$.

(2) Uniform distribution

With the optimisation and improvement of ion thrusters, the beam distribution uniformity is greatly improved[20]. In such a condition, it is more reasonable to assume that beam ions are uniformly distributed in the outlet plane. Therefore, the density of beam ions distributed in the outlet plane is:

$$n_i(r) = A\bar{n}_{bi} \quad \ldots(7)$$

The beam currents in the outlet plane of an ion thruster also shall meet Equation (5). Substitute Equation (7) into Equation (5) and obtain:

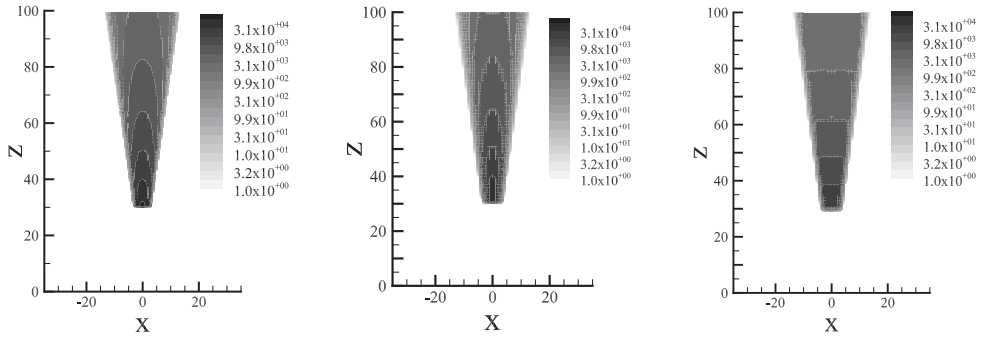
$$I_b = 2Aev_{bi}\bar{n}_{bi}\pi r_0^2 \cdot \left(\frac{\cos\alpha_0 - 1}{{\alpha_0}^2} + \frac{\sin\alpha_0}{\alpha_0}\right) \quad \ldots(8)$$

When $\alpha_o \ll 1$, $\frac{\cos\alpha_0 - 1}{{\alpha_0}^2} + \frac{\sin\alpha_0}{\alpha_0} \approx 0.5$ and $A \approx 1$.

2.3 Comparison of simulation results of beam ions

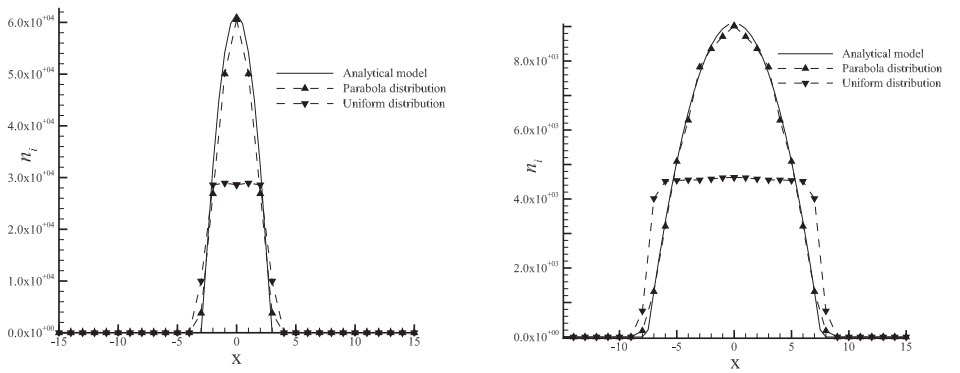
Taking the divergence angle of 7.5° as an example, the beam ion number density distribution of analytical model and the particle model was compared. Figure 3 shows the number density distribution of beam ions of these two models. Figures 4 and 5 show the variation trend comparison of the simulation results of these two models in the axial and radial directions. It can be seen that the particle model with parabola distribution agrees well with the analytical

https://doi.org/10.1017/aer.2018.79 Published online by Cambridge University Press



(a) Analytical model (b) Particle model(parabola) (c) Particle model(uniform)

Figure 3. Comparison of the number density of beam ions.



(a) In the outlet of thruster (b) 20cm from the outlet plane of the thruster

Figure 4. Radial distribution of the number density of beam ions.

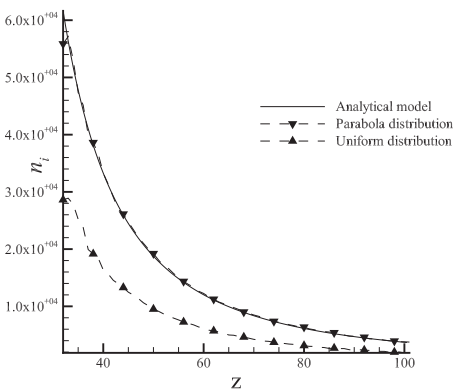


Figure 5. Number density distribution of beam ions in the outlet axis.

https://doi.org/10.1017/aer.2018.79 Published online by Cambridge University Press

model. The simulation results of the particle model in two different distribution modes, the uniform distribution and the parabola distribution have a great difference with each other. Therefore, the analytical model is no longer applicable to the ion thrusters whose beam uniformity is significantly improved.

3.0 CEX ION SIMULATION MODEL

In this section, the simulation method and flow of the generation and tracking of CEX ion are briefly introduced. Then, the analytical model and the 3D particle model were used respectively to obtain the beam ion distribution, the neutral atom distribution and the CEX ion distribution of the NSTAR ion thruster. Finally, the simulation results of these two models were compared with each other to verify the correctness and accuracy of the 3D particle model.

3.1 Introduction of CEX collision model

In addition to the beam ion distribution, the distribution of the neutral atoms of plume should be obtained. In the analytical model, the distribution of neutral atoms still obeys the point source model[5]. In the particle model, the distribution of neutral atoms is obtained by the DSMC method. The detailed description of the DSMC method is shown in the Ref. 6. A common assumption in plume modeling is that electrons are isothermal and electron density can be described by the Boltzmann relationship[7].

Once the distributions of beam ions and neutral atoms are obtained, the generation of the CEX ion can be simulated by the MCC method. For the analytical model, a CEX collision can only be simulated by Standard MCC. In the 3D particle model, two collision methods, Standard MCC and P_null MCC, can be used for the simulation. In order to compare with the analytical model, only the Standard MCC method is used in the 3D particle model in this section. The potential and the particle position tracking of the CEX ion are simulated by IFE-PIC methods.

Hence, the CEX ion simulation process is divided into three steps:

(1) Simulation of beam ions with the analytical model or the particle model.

(2) Simulation of neutral flow exhausted from the ion thruster with the analytical model or the DSMC model.

(3) Simulation of the potential and CEX ions using IFE-PIC-MCC methods and beam ions and neutral flow obtained above, respectively. In the Standard MCC method, the volumetric generation of CEX ions is calculated with the following equation:

$$N_{CEX} = n_n n_i v_{bi} \sigma_{CEX}(v_{bi}), \quad \ldots (9)$$

where n_n is the neutral atom densities and σ is the velocity dependent CEX cross section.

3.2 Numerical simulation setup

Due to the symmetry of the NSTAR satellite, a quarter-symmetry model is employed to simulate CEX ions of the plume of the NSTAR thruster, as shown in Fig. 6. The simulation region is a three-dimensional cuboid domain that includes two cylinders with the potential of −2V. The operational parameters and the experimental data of the NSTAR ion thruster in this section are derived from Ref. 7. The operating condition is ML83. The divergence

https://doi.org/10.1017/aer.2018.79 Published online by Cambridge University Press

Table 1
Operational parameters of the NSTAR ion thruster[7]

Parameters (units)	Numerical values
Voltage U_{acc} (V)	1,095
Beam current I_b (A)	1.4
Divergence angle α_o (°)	15
Ionization rate (%)	88
Radius r_0 (mm)	150
Neutral atom temperature (K)	500
Electron temperature Te (eV)	2

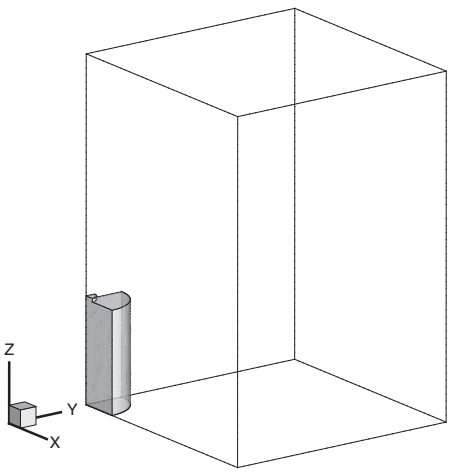


Figure 6. Computational domain.

Table 2
Reference variables

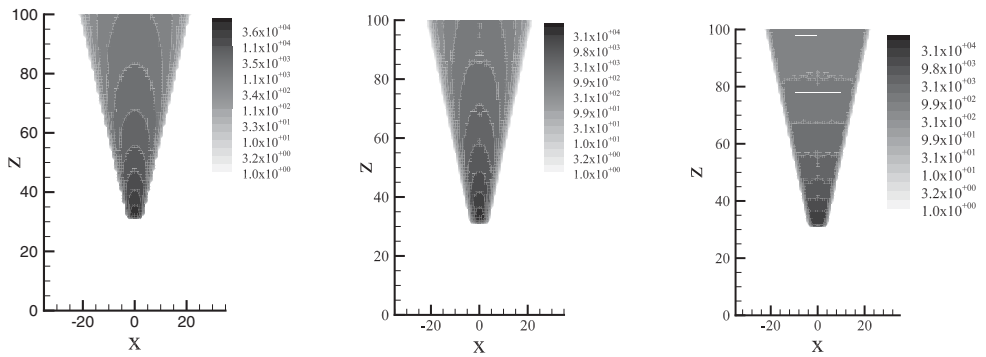
Reference quantity	Reference value
Charge quantity q_{ref}	1.6022×10^{-19} C
Mass m_{ref}	2.18×10^{-25} kg
Length L_{ref}	5.2566×10^{-2}m
Velocity v_{ref}	1,917.4 m/s
Number density n_{ref}	$1.0 \times 10^{11}/\text{m}^3$
Potential Φ_{ref}	5 V
Temperature T_{ref}	5 eV
Permitivity ε_{ref}	$8.85 \times 10^{-12} \cdot \text{m}^{-1}$

angle is 15°. These parameters can be found in Table 1. The reference variables for the plume simulations in this paper are listed in Table 2 and the normalised geometric parameters of the objects in the simulating domain are listed in Table 3. All surfaces satisfy the Neumann boundary condition. The particles that hit the XZ plane and YZ plane are reflected, whereas

https://doi.org/10.1017/aer.2018.79 Published online by Cambridge University Press

Table 3
Normalised geometric parameters

Geometric parameter	Dimensionless quantity
Thruster radius r_0	2.85
Thruster height h_0	1
Satellite radius r_s	12
Satellite height h_s	30



(a) Analytical model (b) Particle model(parabola) (c) Particle model(uniform)

Figure 7. Beam ion simulation results.

those that hit the other four surfaces are absorbed. The number of cells used in the final simulation domain is $70 \times 70 \times 100$.

3.3 Comparison of CEX ion simulation results

Figure 7 shows the simulation results of beam ions. The simulation result of the particle model with the parabola distribution still coincides well with that of the analytical model at the divergence angle of 15°. And the result of the particle model with the uniform distribution still has a great difference with the others.

Figure 8 shows the simulation results of neutral atoms. The simulation results coincide well with each other only in the near-field region. In the far-field region, the neutral atom density of the analytical model is larger than that of the DSMC model. In Ref. 21, Boyd obtained the same result.

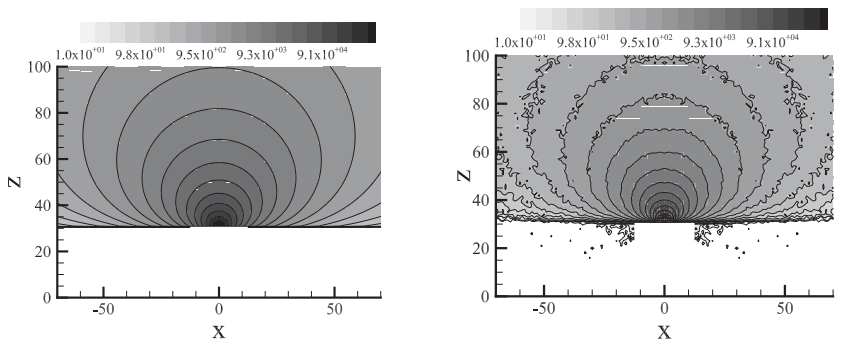
The comparisons of the potential and the CEX ion density distribution between the analytical model and the particle model with the parabola distribution or the uniform distribution are illustrated in Figs 9 and 10. The potential and density distribution of the CEX ion of the particle model is smaller than those of the analytical model. Obviously, this is due to the difference between the simulation results of neutral atoms. However, within the particle model, despite the great difference in the main beam region, the distribution of CEX ions of the uniform distribution is similar with that of the parabola distribution.

Table 4 lists the simulation results and the experimental data. Both the measuring point in the experiment and the observation point in the simulations are in the ion thruster outlet plane with a distance of 75 cm from the outlet axis. The simulation results of the particle model with the parabola distribution are slightly lower than those of the analytical model, but still

https://doi.org/10.1017/aer.2018.79 Published online by Cambridge University Press

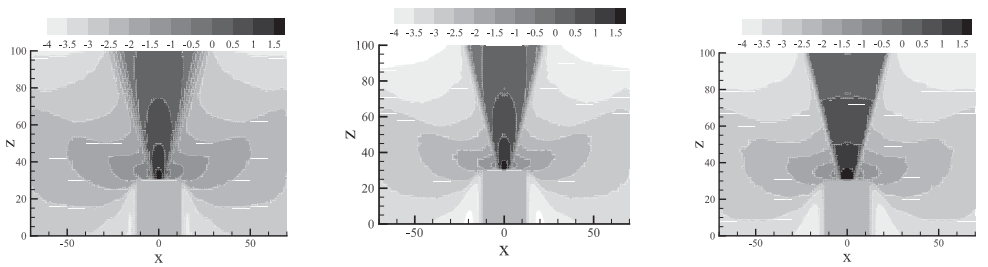
Table 4
Measured value of CEX ion of the NSTART plume

Type ML83	CEX ion density ($10^{12}m^{-3}$)	Current density ($10^{-3}A/m^2$)
Analytical model	1.43	1.49
3D particle model with parabola distribution	1.28	1.07
3D particle model with uniform distribution	0.98	0.82
Measured value	1.2–4.4	0.9–3.3



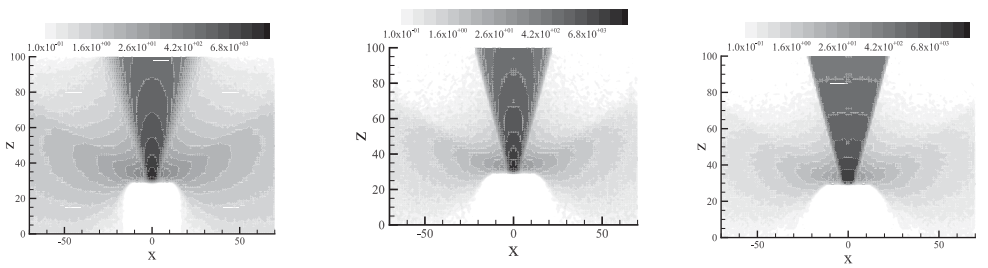
(a) Analytical mode (b) DSMC model

Figure 8. Neutral atom density distribution.



(a) Analytical model (b) Particle model(parabola) (c) Particle model(uniform)

Figure 9. Potential distribution of CEX ions.



(a) Analytical model (b) Particle model(parabola) (c) Particle model(uniform)

Figure 10. Density distribution of CEX ions.

https://doi.org/10.1017/aer.2018.79 Published online by Cambridge University Press

in good agreement with the experimental data. According to Figs. 7 and 8, the reason for this phenomenon is also that the simulation results of neutral atoms of the particle model in the far-field region are smaller than those of the analytical model. However, the results of the particle model with the uniform distribution are smaller than the experimental data.

4.0 SIMULATION RESULTS AND ANALYSIS OF THE ANNULAR ION THRUSTER PLUME

The geometric structure of the annular ion thruster is greatly different from that of the traditional ion thruster but is similar to that of a Hall thruster[8] so that the analytical model is no longer applicable to the simulation of the annular ion thruster plume. Therefore, the 3D particle model is used to simulate the plume of the annular ion thruster in this section, in order to study the characteristics of the plume of the annular ion thruster and illustrate the universality of the 3D particle model as well.

4.1 The 3D particle model for the annular ion thruster plume

In the 3D particle model of the annular ion thruster, CEX collision model is the same as that of the traditional ion thruster exactly. The DSMC model of neutral atoms is basically the same as that of the traditional ion thruster. The only difference is that the exit plane becomes an annular surface.

However, except that the calculation method of v_i is the same as that of the traditional ion thruster, the beam ion particle model of the annular ion thruster has two differences:

(1) Because the beam current has two divergence angles, the inner divergence angle α_i and the outer divergence angle α_o, the initial velocity direction distribution of beam ions is different from that of the traditional ion thruster. As shown in Fig. 11, the initial velocity direction of beam ions can still be expressed as (v_i; α_1; α_2) under the spherical

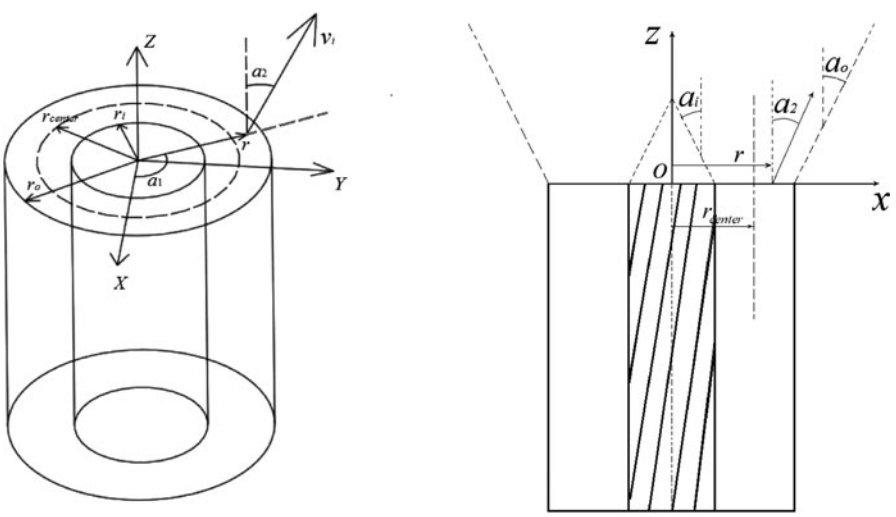


Figure 11. Spherical coordinate description of beam ion velocity of the annular ion thruster.

https://doi.org/10.1017/aer.2018.79 Published online by Cambridge University Press

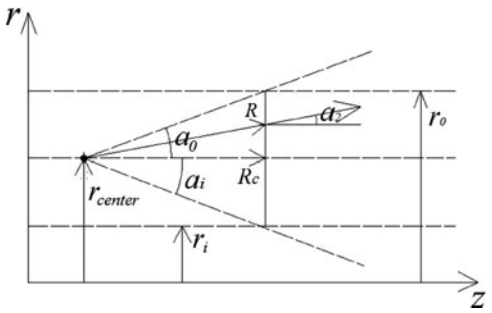


Figure 12. Schematic diagram of point-source model of beam ions of the annular ion thruster.

coordinates and the meanings of α_1 and α_2 are the same as the descriptions in Section II. The difference is that the value of α_2 changes from α_i to α_o:

$$\alpha_2(r) = \begin{cases} \arctan\left(\frac{r_{\text{center}}-r}{r_{\text{center}}-r_i}\tan\alpha_i\right), & r_i \le r < r_{\text{center}} \\ \arctan\left(\frac{r-r_{\text{center}}}{r_o-r_{\text{center}}}\tan\alpha_o\right), & r_{\text{center}} \le r \le r_o, \end{cases} \quad \ldots(10)$$

where r_o is the external radius and r_i is the internal radius of the outlet of the annular ion thruster, and r_{center} is the radius between r_o and r_i, $r_{\text{center}} = \frac{r_i\tan\alpha_o - r_o\tan\alpha_i}{\tan\alpha_o - \tan\alpha_i}$.

(2) The beam uniformity of the annular ion thruster is better than that of the conventional ion thruster, but the beam density at the middle ring is still higher than that at the inner or outer ring in the thruster outlet[22,23].

Therefore, in the simulation for the distribution of beam ions of the annular ion thruster, both the uniform distribution and the parabola distribution are used. In order to find a more reasonable allocation method, their results are compared. The uniform distribution for the annular ion thruster is the same as that of the traditional ion thruster, except $\bar{n}_{bi} = \frac{I_b}{ev_{bi}\pi\left(r_o^2 - r_i^2\right)}$.

There is no corresponding analytical model of the beam ion distribution for the annular ion thruster. Therefore, it is assumed that the beam ion density distribution of the annular ion thruster is also subject to the parabolic distribution and the point-source model, as shown in Fig. 12.

Therefore, the beam ion density distribution in the outlet plane of the annular ion thruster can be constructed according to Equation (1),

$$n_i(r) = \begin{cases} A\bar{n}_{bi}\cos^2(\alpha_2(r))\left(1 - \frac{\alpha_2^2(r)}{\alpha_i^2}\right), & r_i \le r < r_{\text{center}} \\ A\bar{n}_{bi}\cos^2(\alpha_2(r))\left(1 - \frac{\alpha_2^2(r)}{\alpha_o^2}\right), & r_{\text{center}} \le r \le r_o \end{cases} \quad \ldots(11)$$

It is also necessary to set the coefficient A to ensure that the beam current in the annular ion thruster exit is still equal to I_b.

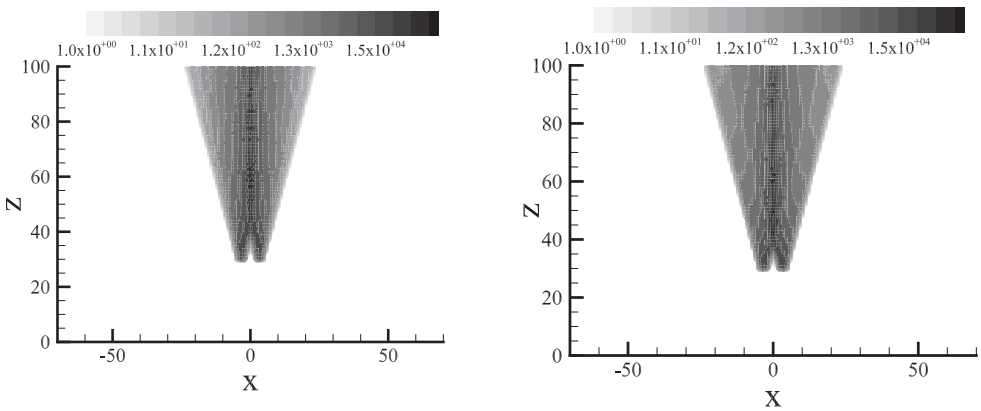
The beam currents in the exit plane of the annular ion thruster shall meet:

$$I_b = \int_{r_i}^{r_o} n_i(\alpha_2(r))ev_{bi}\cos(\alpha_2(r))2\pi r dr \quad \ldots(12)$$

https://doi.org/10.1017/aer.2018.79 Published online by Cambridge University Press

Table 5
Operational parameters of the annular ion thruster

Parameters (units)	Numerical values
Voltage U_{acc} (V)	1,800
Beam current I_b (A)	1.6
Outer divergence angle α_o (°)	15
Inner divergence angle α_i (°)	−15
Ionization rate (%)	90
Outer radius r_o (mm)	225
Inner radius r_i (mm)	126
Neutral atom temperature (K)	500
Electron temperature Te (eV)	2



(a) Particle model(parabola) (b) Particle model(uniform)

Figure 13. Beam ion number density distribution.

Due to the symmetry between the inner divergence angle and the outer divergence angle, it is generally considered that $-\alpha_i = \alpha_o$. Then, substitute the Equation (11) into Equation (12) and obtain:

$$A = \alpha_o{}^2 \tan\alpha_o / (2\sin\alpha_o - 2\alpha_o \cos\alpha_o) \quad \ldots (13)$$

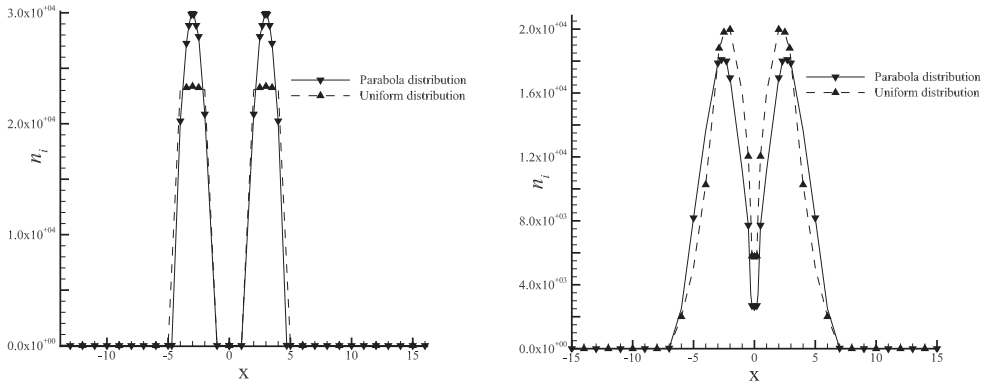
When $\alpha_o \ll 1$,

$$A \approx 1.5 \quad \ldots (14)$$

4.2 Simulation results and analysis

The numerical model setup for the annular ion thruster is the same as the NSTAR ion thruster. And the design parameters of the annular ion thruster are shown in Table 5. Since the inner divergence angle is equal to the outer divergence angle, the coefficient A is set to be 1.5. Figure 13 shows the comparison of beam ion distribution between the parabola distribution

https://doi.org/10.1017/aer.2018.79 Published online by Cambridge University Press



(a) Outlet of thruster (b) 20cm at the downstream thruster

Figure 14. Radial distribution of beam ion number density

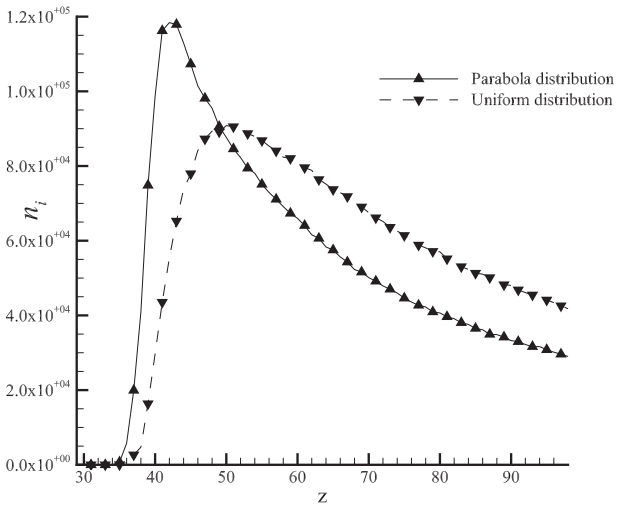


Figure 15. Distribution of beam ion number density in the outlet axis.

and the uniform distribution. It can be seen that the distribution of beam ions of the annular ion thruster changes greatly compared with that of the traditional ion thruster. The beam currents are overlapped in the axis area, so the beam density is higher in the axis region than in the wing area. The layering of the beam ion density along the axis direction is not obvious. From Fig. 13(a) and (b), it can be seen that the overall ion density distribution of the uniform distribution is quite similar with that of the parabola distribution. Figure 14 shows the radial distribution of the density of beam ions. It can be seen that the radial distribution of beam ions of the annular ion thruster in the near-field region presents an M-shape. Figures 14 and 15 illustrate that the difference in the radial or axial directions between these two modes of distribution is not very large. Hence, the simulation results of beam ions are almost the same.

Figure 16 shows the simulation result of neutral atoms of the annular ion thruster. It is not far from that of the traditional ion thruster. Figures 17 and 18 show CEX ion distribution of the annular ion thruster with different allocation method. The distributions of CEX ions are

https://doi.org/10.1017/aer.2018.79 Published online by Cambridge University Press

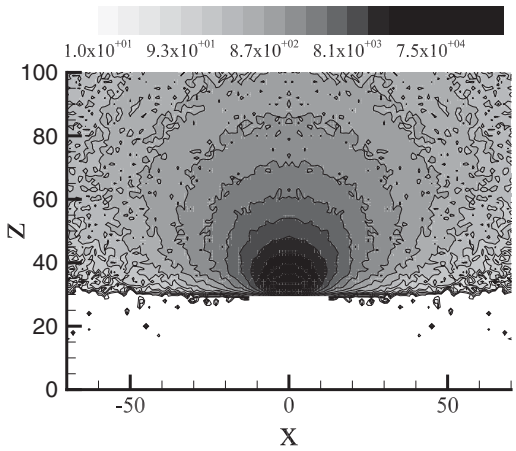
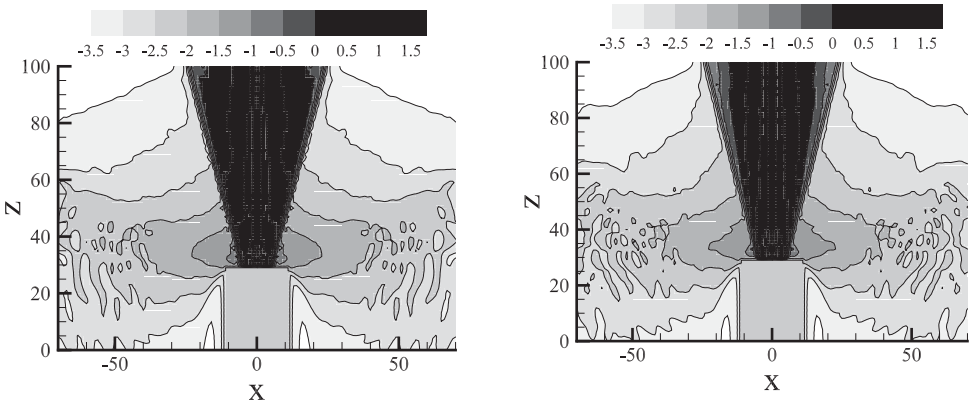
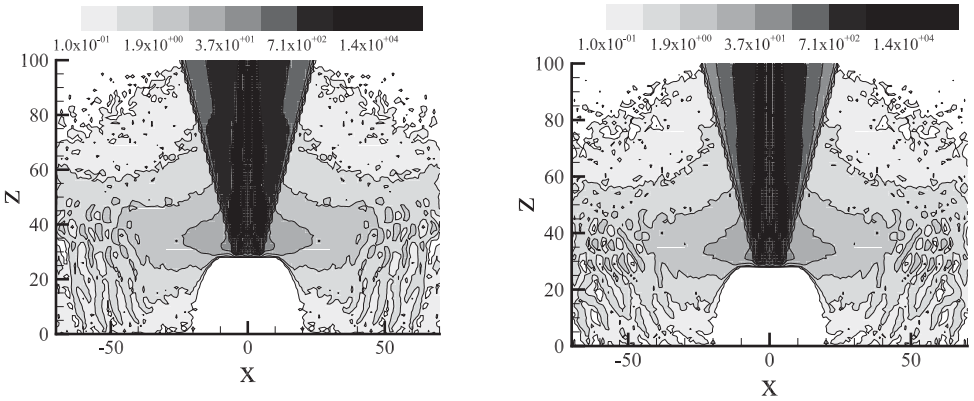


Figure 16. Neutral atom density distribution.



(a) Parabola distribution (b) Uniform distribution

Figure 17. Potential distribution of CEX ions of the annular ion thruster.



(a) Parabola distribution (b) Uniform distribution

Figure 18. Density distribution of CEX ions of the annular ion thruster.

https://doi.org/10.1017/aer.2018.79 Published online by Cambridge University Press

basically the same due to the similarity in beam ion distributions of the uniform and parabola distribution modes. But they have a great difference with those of the traditional ion thruster. The potential and density distribution of CEX ions in the near-field region exhibit a wave-like look. This is because the beam ion distribution in the near-field region is in the M-shape with a high-low conversion in the radial direction so that the distribution of CEX ions diffused from the near-field region becomes wave-like eventually.

5.0 CONCLUSION

In this paper, a 3D Particle model with two modes of initial distribution, the parabola distribution based on the analytical model and the uniform distribution, is proposed. The CEX ion simulation results of the particle model with parabola distribution of the NSTAR ion thruster show that the simulation results coincide well with the experimental data and those of the analytical model, illustrating that with a reasonable initial distribution, the 3D particle model can simulate the plume of a traditional ion thruster well.

The simulation results of the annular ion thruster show that the beam ion distribution of the annular ion thruster changes greatly compared with that of the traditional ion thruster. The number density of beam ions is high in the axis area but low in the wing area. In addition, it presents an M-shape in the radial direction in the near-field region. In the 3D particle model of the annular ion thruster, the DSMC model and the CEX collision model are basically the same as those of the traditional ion thruster. Hence, the reason for the quite different CEX ion distribution of the annular ion thruster is the large difference in the beam ion distribution. However, the simulation results of beam ions in the uniform and parabola distribution modes are almost the same with each other. Due to the beam ion distribution similarity of the uniform and parabola distribution modes of the annular ion thruster, the distributions of CEX ions obtained by these two modes are similar as well.

ACKNOWLEDGEMENTS

This work was supported by the Open fund for National Key Laboratory of Science and Technology on Vacuum Technology and Physics under Contract No. ZWK1607 and the program of Shenzhen Technology Projects (JCYJ20170413103337899, JCYJ20160226201347750).

REFERENCES

1. SAMANTA ROY, R.I., HASTINGS, D.E. and GATSONIS, N.A. Modelling of ion thruster plume contamination, 30th AIAA/ASME/SAE/ASEE Joint Propulsion Conference & Exhibit, 27-29 June, Indianapolis, Indiana, US, AIAA 1994-3138.
2. STEPHANI, K.A., BOYD, I.D., BALTHAZOR, R.L., MCHARG, M.G., UELLER, B.A. and ADAMS, R.J. Analysis and observation of spacecraft plume/ionosphere interactions during maneuvers of the space shuttl, *J Geophysical Research: Space Physics*, 2014, **119**, (9), pp 7636-7648.
3. KING, L.B., PARKER, G.G., DESHMUKH, S. and CHONG, J.H. Study of interspacecraft coulomb forces and implications for formation flying, *J Propulsion and Power*, 2003, **19**, (3), pp 497-505.
4. SHAN, K., CHU, Y., LI, Q., ZHENG, L. and CAO, Y. Numerical Simulation of Interaction between Hall Thruster CEX Ions and SMART-1 Spacecraft, *Mathematical Problems in Engineering*, **2015**, (3), pp 1-8.
5. SAMANTA ROY, R.I. Numerical simulation of ion thruster plume backflow for spacecraft contamination assessment, *Massachusetts Institute of Technology*, 1995.

https://doi.org/10.1017/aer.2018.79 Published online by Cambridge University Press

6. BIRD, G.A. Molecular gas dynamics and the direct simulation Monte Carlo of gas flows, *Clarendon, Oxford*, 1994, **508**, p 128.
7. WANG, J., BRINZA, D. and YOUNG, M. Three-dimensional particle simulations of ion propulsion plasma environment for deep space 1t, *J Spacecraft and Rockets*, 2001, **38**, (3), pp 433-440.
8. PATTERSON, M.J., HERMAN, D., SHASTRY, R., NOORD, J.V. and FOSTER, J.E. Annular-geometry ion engine: Concept, development status, and preliminary performance, 48th AIAA/ASME/SAE/ASEE Joint Propulsion Conference & Exhibit, 30 July-1 August, Atlanta, Georgia, US, AIAA 2012-3798.
9. HAN, D. and WANG, J.J. Simulations of ion thruster plume contamination with a whole grid sputtered Mo source model, 49th AIAA/ASME/SAE/ASEE Joint Propulsion Conference & Exhibit, 14-17 July, San Jose, California, US, AIAA 2013-3888.
10. WANG, J., HAN, D. and HU, Y. Kinetic simulations of plasma plume potential in a vacuum chamber, *IEEE Transactions on Plasma Science*, 2015, **43**, (9), pp 3047-3053.
11. TAJMAR, M., GONZALEZ, J. and HILGERS, A. Modeling of spacecraft-environment interactions on SMART-1, *J Spacecraft and Rockets*, 2001, **38**, (3), pp 393-399.
12. MARKELOV, G. and GENGEMBRE, E. Modeling of plasma flow around SMART-1 spacecraft, *IEEE Transactions on Plasma Science*, 2006, **34**, (5), pp 2166-2175.
13. BOYD, I.D. Numerical simulation of Hall thruster plasma plumes in space, *IEEE Transactions on Plasma Science*, 2006, **34**, (5), pp 2140-2147.
14. KAFAFY, R. and CAO, Y. Modelling ion propulsion plume interactions with spacecraft in formation flight, *The Aeronautical J*, 2010, **114**, (1157), pp 417-426.
15. KAFAFY, R., LIN, T., LIN, Y. and WANG, J. Three-dimensional immersed finite element methods for electric field simulation in composite materials, *Int J Numerical Methods Engineering*, 2005, **64**, (7), pp 940-972.
16. WANG, J., CAO, Y., KAFAFY, R., PIERRU, J. and DECYK, V.K. Simulations of ion thruster plume–spacecraft interactions on parallel supercomputer, *IEEE Transactions on Plasma Science*, 2006, **34**, (5), pp 2148-2158.
17. WANGY, J., CAO, Y., KAFAFY, R. and DECYK, V.K. Electric propulsion plume simulations using parallel computer, *Scientific Programming*, 2007, **15**, (2), pp 83-94.
18. SAMANTA ROY, R.I., HASTINGS, D.E. and GASTONIS, N.A. Ion-thruster plume modeling for backflow contamination, *J Spacecraft and Rockets*, 1996, **33**, (4), pp 525-534.
19. DAVID, O., BENSON, S., WITZBERGER, K. and CUPPLES, M. Deep space mission applications for NEXT: NASA's evolutionary xenon thrusterr, 40th AIAA/ASME/SAE/ASEE Joint Propulsion Conference & Exhibit, 11-14 July, Fort Lauderdale, Florida, US, AIAA 2004-3806.
20. SHASTRY, R., HERMAN, D.A., SOULAS, G.C. and PATTERSON, M.J. Status of NASA's Evolutionary Xenon Thruster (NEXT) Long-Duration Test as of 50,000 h and 900 kg Throughput, 33rd International Electric Propulsion Conference, IEPC-2013-121, Washington, DC, US, 6-10 October 2013.
21. BOYD, I.D., VAN GILDER, D.B. and LIU, X. Monte Carlo simulation of neutral xenon flows in electric propulsion devices, *J Propulsion and Power*, 1998, **14**, (6), pp 1009-1015.
22. SHASTRY, R., PATTERSON, M.J., HERMAN, D.A. and FOSTER, J.E. Current density measurements of an annular-geometry ion engine, 48th AIAA/ASME/SAE/ASEE Joint Propulsion Conference & Exhibit, 30 July-1 August, Atlanta, Georgia, US, AIAA 2012-4186.
23. PATTERSON, M.J., FOSTER, J.E., YOUNG, J.A. and CROFTON, M.W. Annular engine development status, *AIAA Paper*, 2013, **3892**.

https://doi.org/10.1017/aer.2018.79 Published online by Cambridge University Press